Clays and Clay Minerals, Vol. 34, No. 5, 511–520, 1986.

ION EXCHANGE, THERMAL TRANSFORMATIONS, AND OXIDIZING PROPERTIES OF BIRNESSITE

D. C. GOLDEN, J. B. DIXON, AND C. C. CHEN

Department of Soil & Crop Sciences, Texas A&M University
College Station, Texas 77843

Abstract—Synthetic sodium birnessite, having a cation-exchange capacity (CEC) of 240 meq/100 g (cmol/kg) was transformed into Li, K, Mg, Ca, Sr, Ni, and Mn^{2+} cationic forms by ion exchange in an aqueous medium. Competitive adsorption studies of Ni and Ba vs. Mg showed a strong preference for Ni and Ba by birnessite. The product of Mg^{2+}-exchange was buserite, which showed a basal spacing of 9.6 Å (22°C, relative humidity (RH) = 54%), which on drying at 105°C under vacuum collapsed to 7 Å. Of the cation-saturated birnessites with 7-Å basal spacing, only Li-, Na-, Mg-, and Ca-birnessites showed cation exchange.

Heating birnessite saturated with cations other than K produced a disordered phase between 200° and 400°C, which transformed to well-crystallized phases at 600°C. K-exchanged birnessite did not transform to a disordered phase; rather a topotactic transformation to cryptomelane was observed. Generally the larger cations, K, Ba, and Sr, gave rise to hollandite-type structures. Mn- and Ni-birnessite transformed to bixbyite-type products, and Mg-birnessite (buserite) transformed to a hausmannite-type product. Li-birnessite transformed to cryptomelane and at higher temperature converted to hausmannite. The hollandite-type products retained the morphology of the parent birnessite. The mineralogy of final products were controlled by the saturating cation. Products obtained by heating natural birnessite were similar to those obtained by heating birnessite saturated with transition elements.

Key Words—Birnessite, Bixbyite, Buserite, Cation exchange, Cryptomelane, Hausmannite, Hollandite, Oxidation, Thermal treatment.

INTRODUCTION

Birnessite is one of the most common manganese oxides in the clay-size fraction (<2 μm) of soils. It has been identified in soil concretions in Australia (Taylor *et al.*, 1964) and the Soviet Union (Chukhrov and Gorshkov, 1981). Manganese minerals of this type are an important source of nutrient Mn. In addition, the relatively soluble nature of these minerals under waterlogged or extremely acid conditions may contribute to Mn toxicity in many plants. The cation-exchange preference of birnessite for heavy metals makes it important from a pollution-abatement point of view and in controlling the availability of certain trace elements, some of which are essential to plants and animals (e.g., Co and Cu). Adams *et al.* (1969) showed that the availability of cobalt to plants is controlled to a large extent by the amount of manganese in the soil.

The chemistry, structure, and other properties of natural birnessite and its cation-exchange derivatives, however, are not well understood. Its structure is thought to be similar to that of chalcophanite (Burns and Burns, 1977), although a precise determination has not been made. The structure probably consists of sheets of water molecules between sheets of edge-sharing MnO_6 octahedra, the arrangement being repeated about every 7.2 Å along the *c*-axis. One of six octahedral sites in the MnO_6 octahedra is unoccupied, and Mn^{2+} and Mn^{3+} lie above and below each octahedral vacancy. These low-valence Mn ions are coordinated to oxygens in both the octahedral MnO_6 sheet and the water sheet (Figure 1). Synthetic birnessite was reported to be non-stoichiometric (Giovanoli *et al.*, 1973), the formula for the sodium form being $Na_4Mn_{14}O_{26}\cdot 9H_2O$ and the sodium-free form, $Mn_7O_{13}\cdot 5H_2O$ (Giovanoli *et al.*, 1970).

To increase our understanding of the behavior of birnessite in the soil system, synthetic birnessite was characterized by X-ray powder diffraction, chemical, and infrared spectroscopic techniques. The cation-exchange properties and the thermal stabilities of various exchanged products were also investigated and compared with those of the natural material.

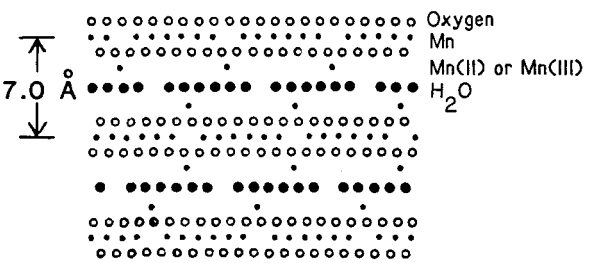

Figure 1. Birnessite structure modeled after chalcophanite (after Burns and Burns, 1977) as seen in a section perpendicular to the *b*-axis.

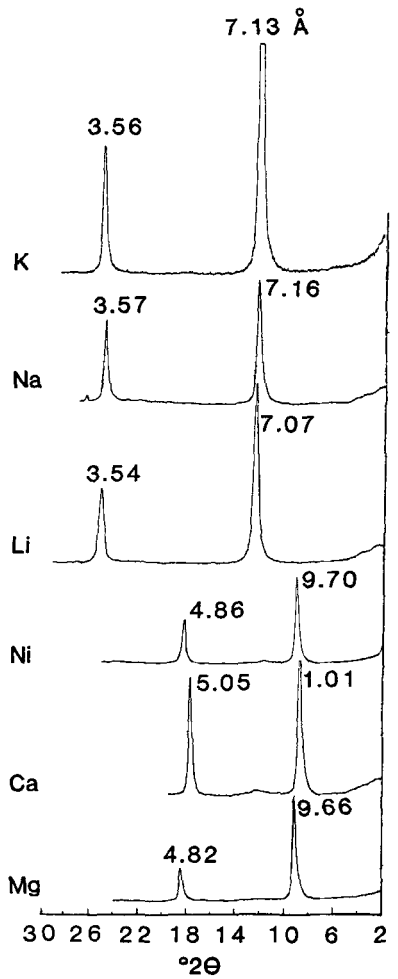

Figure 2. Basal spacings (in Å) of birnessite saturated with K, Na, Li, Ni, Ca, and Mg (22°C, relative humidity = 54%, CuKα radiation).

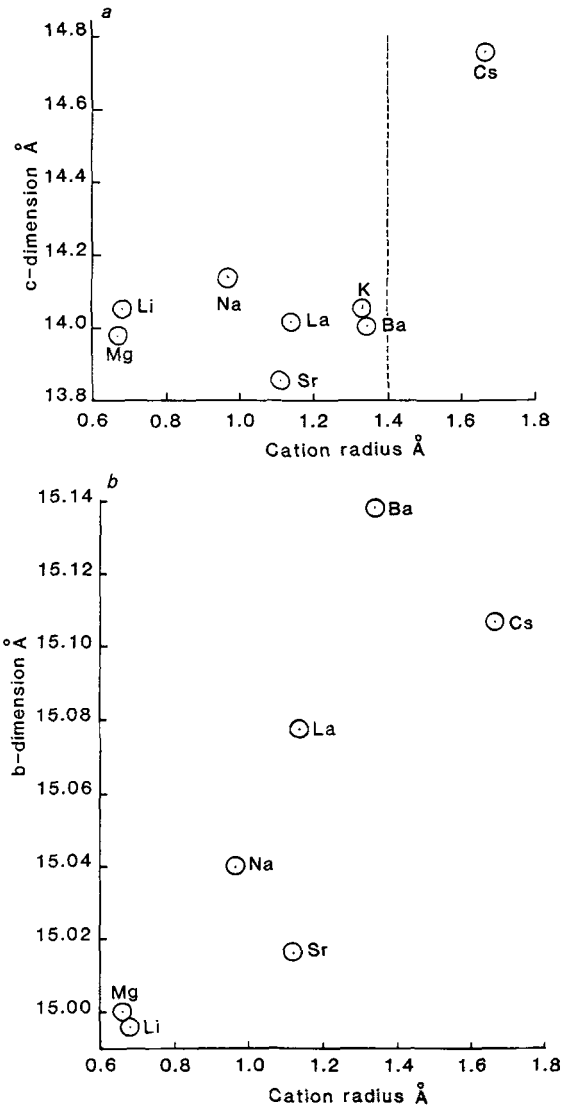

Figure 3. (a) Plot of c dimension vs. cation radius for cation-saturated birnessite samples after heating at 105°C under vacuum for 24 hr (dotted line at 1.4 Å denotes ionic radius of oxygen). (b) Plot of b dimension (calculated from d(060)) vs. cation radius for cation-saturated birnessite heated at 105°C under vacuum for 24 hr.

EXPERIMENTAL

Synthesis and cation exchange

Birnessite was synthesized by dehydrating buserite prepared by the method of Stähli (1968) in which a solution of 55 g of NaOH in 250 ml H_2O was added to 200 ml of 0.5 M $MnCl_2$ at room temperature (22°C) in a plastic beaker. Oxygen was then bubbled at a rate $\geq$1.5 liter/min through a glass frit into the $Mn(OH)_2$ suspension. After 5 hr of oxygenation the black precipitate of buserite was washed with deionized water. The product was freeze-dried and stored (evacuation during freeze drying dehydrates the buserite to form birnessite; Giovanoli and Brutsch, 1979).

The synthetic birnessite was saturated with Li, K, Mg, Ca, Ba, and Ni by shaking 25-mg portions of Na-birnessite for 17 hr with 20 ml of 1 N chloride solution of the corresponding cation. The pH of the salt solution was 5.5. Excess salt was removed by washing the sample with distilled water during centrifugation. The exchanged birnessites were then mounted on glass slides as a water dispersion for X-ray powder diffraction analysis.

Cation-exchange capacities were determined on freeze-dried samples as follows: 25-mg samples were weighed into 40-ml centrifuge tubes, saturated with K^+, and washed free of excess salt as above. The whole sample was digested with 2 ml of 12 M HCl and 4 ml of 0.1 N $NH_2OH \cdot HCl$ solution. Total K in the digestate was determined by atomic absorption spectrometry. CECs were calculated on the basis of total K meq/100 g of sample.

Competitive adsorption isotherms of Ba vs. Mg and Ni vs. Mg were determined using the procedure of Weed and Weber (1968). Alkylammonium ion saturation for layer charge determination was performed by the method of Lagaly and Weiss (1969), as modified by Ruehlicke and Kohler (1981).

X-ray powder diffraction and infrared analysis

X-ray powder diffraction (XRD) analysis was performed by using a Philips Norelco X-ray diffractometer equipped with

https://doi.org/10.1346/CCMN.1986.0340503 Published online by Cambridge University Press

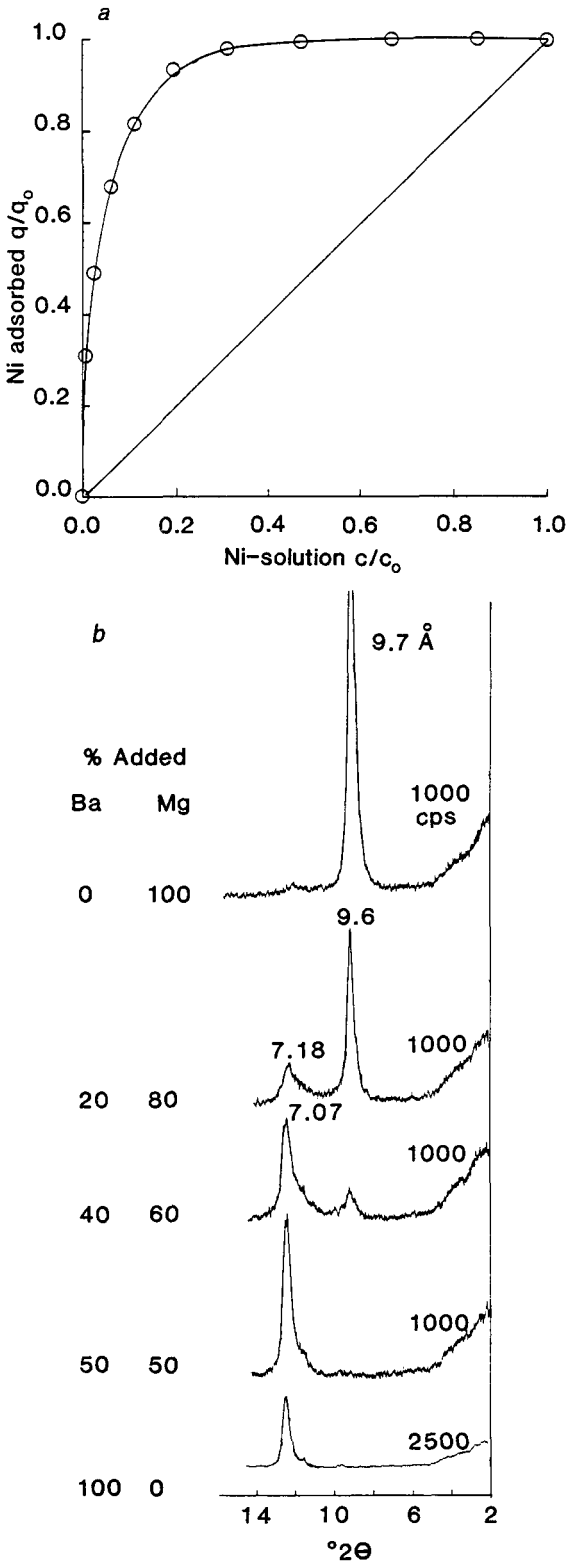

Figure 4. (a) Competitive adsorption isotherm of Ni^{2+} vs. Mg^{2+}. C = concentration of Ni^{2+} in solution; C_0 = total cationic (Ni + Mg) concentration in solution; q = Ni in adsorbed phase (mole/g); q_0 = total cations in adsorbed phase. (b) X-ray powder diffraction patterns for samples of birnessite exposed to different molar ratios of Ba^{2+}:Mg^{2+} in solution (CuKα radiation).

Table 1. Infrared absorption bands of cation-saturated birnessite.

Saturating cation	Infrared bands (cm^{-1})					
Li	633	511	480	427	364	226
Na	633	512	480	421	359	227
K	626	513	482	419	369	225
Mg	625	512	483	427	360[1]	227
Sr	631	514	487	424	365	227
Ba	633	514	483	421	364	226
Ni	630[1]	509	487	421[1]	375[1]	227
Mn	630[1]		497[2]	455[1]	340[1]	227

[1] Broad weak band or shoulder.
[2] Merged 510- and 480-cm^{-1} bands.

Table 2. Major crystalline phases obtained by heating birnessite saturated with cations.

Saturating cation	Octahedral ionic radius[1] (Å)	Phases identified at temperature[2]			
		200°C	400°C	600°C	800°C
K	1.33	B	B	C	C
Ba	1.34	Dis. B	H*	H	H
Sr	1.12	Dis. B	H*	H	H
Ni	0.69	B	Dis. B	Bix	Bix
Mg	0.66	B	Dis. B	Hau	Hau
Li	0.68	Dis. B	C*	C	Hau
Mn^{2+}	0.80	Dis. B	Dis. B	Bix	Bix

[1] Mason and Berry (1968).
[2] B = birnessite, $M_4Mn_{14}O_{27}\cdot 9H_2O$ (M = monovalent metal ion); C = cryptomelane; H = hollandite; Dis. B = disordered birnessite; * = poorly crystalline; Bix = bixbyite; Hau = hausmannite.

a graphite monochromator, using CuKα radiation on oriented mounts of birnessite saturated with Na, K, Mg, Mn^{2+}, Ni, and Ba. The mounts were heated for 2 hr at 200°, 400°, 600°, and 800°C in a stepwise fashion, and XRD patterns were obtained after each heating step. The samples heated at 800°C were mounted on a holey carbon grid and examined by transmission electron microscopy using a Zeiss 10C electron microscope.

Slow XRD scans (¼°/min) of unoriented birnessite saturated with various cations were obtained for the d values of the 002, 004, and 060 reflections. The measurements were repeated after the samples were heated to 105°C under vacuum. XRD analyses were made in triplicate, and average measurements were taken for 2θ values corresponding to each peak. The c and b dimensions of the birnessite unit cell were calculated using these values.

Birnessites saturated with different cations were examined by infrared spectroscopy (IR) by pressing pellets with anhydrous KBr (0.3 mg birnessite/300 mg KBr) at 1.38×10^5 kPa for 5 min. IR spectra were recorded using a Perkin Elmer 283 IR spectrometer equipped with a Model 3600 data station.

https://doi.org/10.1346/CCMN.1986.0340503 Published online by Cambridge University Press

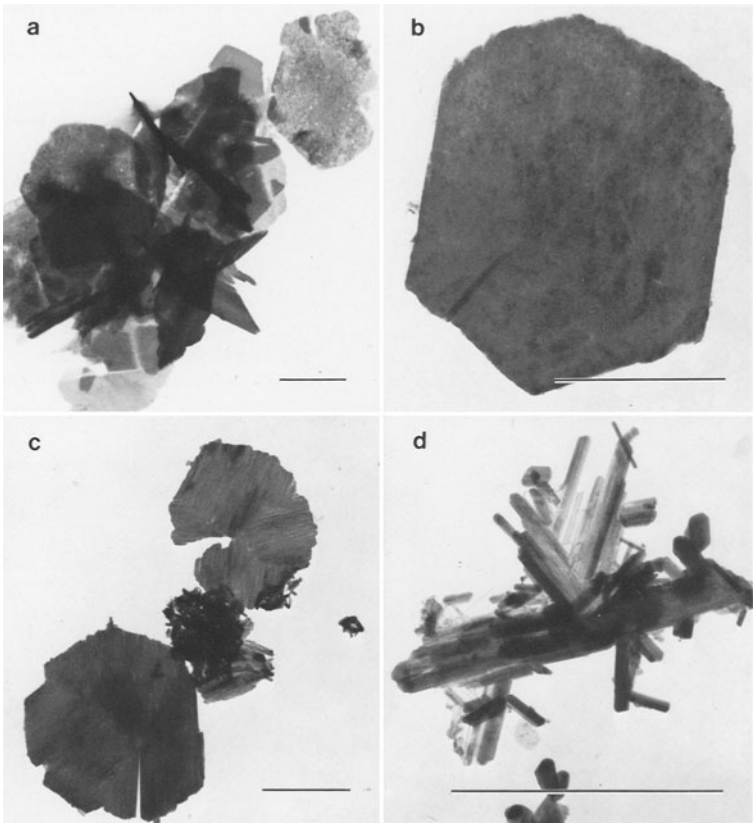

Figure 5. Transmission electron micrographs of: (a) synthetic birnessite showing a variety of morphologies (bar represents 1 μm); (b) hexagonal plate morphology of birnessite; (c, d) barium-saturated birnessite heated to 800°C; (e) nickel-saturated birnessite heated to 800°C; (f) magnesium-saturated birnessite heated to 800°C; (g) potassium-saturated sample heated to

RESULTS AND DISCUSSION

Cation exchange

The synthetic sodium birnessite (freeze dried) gave an XRD pattern similar to that reported by Giovanoli *et al.* (1970). Na-birnessite was easily transformed to other cationic forms by cation-exchange reactions in solution. The interlayer spacing at RH = 54% was dependent on the saturating cation: Na-birnessite had a basal spacing of 7.16 Å (vacuum dried, 7.07 Å); Li-birnessite had a spacing of 7.07 Å; Ni- and Mg-saturated samples had basal spacings of 9.70 and 9.66, respectively, indicating the hydration of birnessite to buserite. Na- or Mg-birnessites in the hydrated form were easily converted to other cationic forms (Li, Na, K, Mg, Ca, Sr, Ni, and La) that displayed either 7- or 10-Å basal spacings (Figure 2). In general, the expanded form which had a spacing of about 9.5–10 Å was easily ion exchanged. Heating samples at 105°C for 12 hr under vacuum, collapsed all the samples to 7 Å and reduced the replaceability of cations by Mg as determined by the appearance of a 10-Å phase. K, Sr, and La showed no exchange, whereas Li, Na, Ca, and Ni indicated exchange by Mg^{2+}. Prolonged heating at 105°C, however, markedly reduced the exchangeability of even these ions.

The 7-Å spacing (002) indicates a single layer of water between octahedral sheets. Birnessite may have rehydrated during the XRD examination because no effort was made to keep the samples dehydrated while they were on the goniometer stage. Of the cations used, only Cs is larger than water and is reflected by the increased *c* dimension (Figure 3a). Slight, but significant differences in *b*-dimension (calculated from d(060)) were observed (Figure 3b) for the heated samples. The *b*-dimension increased from Li to Na to Cs for alkali cations and from Mg to Sr to Ba for alkaline earth cations. No 060 reflection was noted for K-birnessite. In general, *b*-dimension increased with an increase in cation size for both series of cations. The reason for the increase in the *b*-dimension is not clear; however, the smaller cations have larger ionic potentials (charge/radius) and are more effective in layer-charge neutralization. Therefore, an expansion in *b*-dimension may be expected as the cation size increases.

The total CEC of Na-birnessite was 240 meq/100 g,

https://doi.org/10.1346/CCMN.1986.0340503 Published online by Cambridge University Press

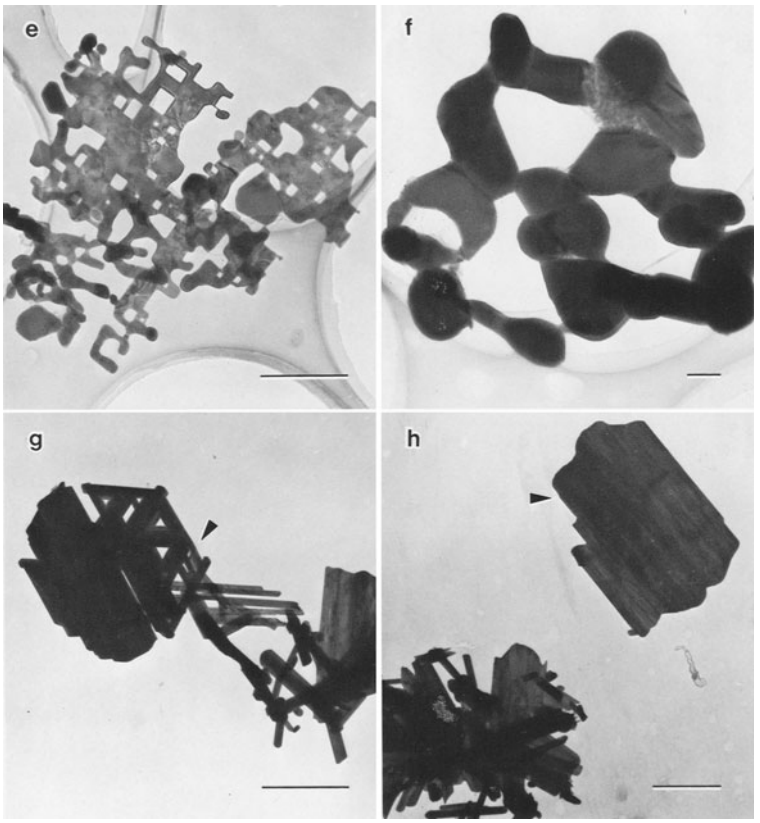

800°C showing well-formed needles of cryptomelane; (h) potassium-saturated sample heated to 800°C showing residual birnessite plate morphology (arrow).

indicating a high layer-charge density. Some cations were adsorbed more strongly than others, as seen from competitive adsorption isotherms. Ni and Ba were strongly preferred over Mg on birnessite (Figures 4a and 4b). The strong preference for transition metal cations such as Ni was in accord with that observed for soil manganese oxides by McKenzie (1967) and Loganathan and Burau (1973) for synthetic δ-MnO_2. Ca and Mg were easily exchanged with other cations. The natural manganese oxide samples often contain Co, Ni, and Ba in appreciable quantities (McKenzie, 1967, 1986). The birnessite in natural samples exhibited no ion exchange either due to such fixed cations or due to chemical changes undergone during dehydration periods.

The birnessites produced by competitive adsorption of Mg and Ba showed two basal XRD reflections at 9.7 and 7.1 Å (Figure 4b). The 7.1-Å peak was due to Ba-birnessite, and the 9.7-Å peak was due to Mg-birnessite. Both the Ba and Mg saturated end members showed more intense peaks than the intermediate compositions (Figure 4b). Also, the selectivity could easily be seen from XRD patterns. Predominantly, Ba-birnessite could be observed from the 20–100% Ba range, but Mg-birnessite only from the 60–100% Mg range; however, a small peak near 7.3 Å was observed in the 100% Mg-saturated sample, indicating a trace of a nonexpandable phase. Small peaks were observed in the Ni-saturated sample (Figure 2) and the Ba-saturated sample at 7.6 Å.

Infrared spectra were not affected by the nature of the nontransition element cations (bands near 630, 511, 480, 427, and 360 cm^{-1}, Table 1). An absorption band near 3400 cm^{-1} (not shown) probably corresponds to stretching of water hydroxyl involved in hydrogen bonding to the surface oxygen and to other water molecules (Farmer, 1974), because the charge produced in the octahedral sheet of MnO_6 is distributed partly on surface oxygens. The interlayer water molecules can hydrogen bond to these surface oxygens giving rise to a IR maximum near 3400 cm^{-1}. A similar IR absorption band was observed for vermiculites (Farmer, 1974). Mn^{2+} and Ni^{2+} seemed to interact differently with the layer structure compared to alkali and alkaline earth cations. Probably Mn and Ni ions exchange with structural Mn or hydrolyze. The interaction of Ni and Mn with the birnessite structure is shown by broad small bands near 630, 420, and 375 cm^{-1} for Ni and 630,

https://doi.org/10.1346/CCMN.1986.0340503 Published online by Cambridge University Press

497, 455, and 340 cm^{-1} for Mn, which were well defined and sharp for Na-birnessite. The IR spectrum of natural birnessite (Potter and Rossman, 1979) has two bands near 500 and 420 cm^{-1} that are diagnostic of birnessite and that are present in all of the samples of different cation saturations. Thus, ion exchange did not affect the mineralogy of the birnessite. The IR spectrum for synthetic Na-birnessite matches well with that reported by Potter and Rossman (1979).

Thermal stability of cation-saturated birnessite

The type of exchange cation influenced the thermal stability of birnessite also. The diversity of crystalline products obtained by heating cation-saturated birnessite to 200°, 400°, 600°, and 800°C is illustrated by the XRD data presented in Figures 6a–6d and Table 2. The nature of these products depended on the type (alkali metal, alkaline earth, transition metal) and radius of the exchange cation. The products of heating various exchanged birnessites to 600°C were cryptomelane, hollandite, hausmannite, and bixbyite. Large cations (Ba, K, etc.) gave rise to hollandite or cryptomelane in concurrence with Giovanoli and Balmer (1981), whereas smaller cations (Li, Mg, etc.) gave rise to bixbyite or hausmannite (Table 2). It is noteworthy that Li-birnessite formed a cryptomelane-like phase at 600°C (not shown) which readily transformed to hausmannite at 800°C. Lithium is a much smaller cation than potassium or barium, yet it caused the formation of a cryptomelane-like phase, however, the product was not heat-stable like that produced from K-birnessite. The two transition metal cations Mn^{2+} and Ni^{2+} gave rise to bixbyite wherein Mn was in a lower valence state (Mn^{3+}) than the parent birnessite (mostly Mn^{4+}). Transformations of the layered mineral birnessite into hausmannite, bixbyite, and hollandite apparently took place via a disordered state (Figure 6, Table 2), which was produced at relatively low temperatures (200°–400°C). Potassium-saturated birnessite (Figure 6a) was stable to 400°C; cryptomelane peaks first appeared at 600°C. At 800°C mostly cryptomelane peaks were evident.

Transmission electron micrographs of the birnessites heated to 800°C showed mainly lath-shaped crystals which appeared to break apart as the transformation proceeded from the original birnessite structure. Some birnessite particles in different intermediate stages of alteration were also present (Figures 5g and 5h). Barium-saturated samples were the most unstable, as evidenced by broad hollandite peaks in the XRD pattern even after the sample had been heated to 400°C (Figure 6b). With increased temperatures, as high as 600°C, Ba-birnessite yielded a well-defined, moderately intense XRD pattern for hollandite. At 800°C, additional peaks for hausmannite were evident, distinct from hollandite peaks. Hausmannite probably formed by the decomposition of birnessite wherein oxygen was lost:

$$Mg_2Mn_{14}O_{27}\cdot 9H_2O \xrightarrow{\text{heat}} 7\ Mn_2O_3 + 2\ O_2 + 9\ H_2O + 2\ MgO. \quad (1)$$

Strontium-saturated samples (Table 2) behaved similarly to the Ba-saturated sample, except that the XRD peaks of the heated products were weak (not shown). An intense peak at 4.07 Å in the XRD pattern of the sample heated to 800°C was probably due to the formation of some cristobalite in the Vycor glass slide at the contact between the sample and the slide. Impurities are known to stabilize the cristobalite structure (Wilding *et al.*, 1977). Heated Mn-oxide or SrO ejected from the sample appeared to catalyze the formation of cristobalite.

Ni- and Mn-saturated birnessite also transformed to bixbyite at 800°C (Table 2); however, the unheated Ni-saturated sample showed a 9.92-Å basal spacing (RH = 54%), in contrast to the 7.19-Å spacing of the Mn-saturated sample. The basal spacing of the Ni-saturated sample (Figure 6d) decreased to 6.89 Å at 200°C; this material seemed to be slightly more stable than Mn-birnessite, which showed much weaker peaks after heating (not shown). In general, the transition metal ions behaved similarly.

The Mg-saturated sample (Figure 6b) behaved similarly to the Ni-saturated sample (Figure 6d) below 400°C. At 600°C Mg-birnessite formed hausmannite, and when the sample was heated at 800°C, the XRD pattern intensified. Li-saturated birnessite upon heat treatment showed a cryptomelane-type pattern below 600°C and at 800°C formed hausmannite. Mg and Li have similar ionic radii; both formed hausmannite as a major product.

The original birnessite was generally pseudohexagonal regardless of the saturating cation (Figures 5a and 5b). The platy crystals were commonly textured and thin. The heated products were thicker, smoother, and commonly twinned (Figures 5c, 5d, and 5g). K- and Ba-birnessites transformed by heating to the tunnel-structured phases, cryptomelane and hollandite, and exhibited laths that are common to those minerals (Figures 5d, 5g, and 5h). Where the platy grains persisted, they were cracked, and textural differences were noted within particles suggesting twinning (Figure 5c). Ni- and Mg-birnessites were transformed by heating to the lower valent oxides of Mn, bixbyite and hausmannite, respectively. Bixbyite and hausmannite are cubic (Embrey and Fuller, 1980) or pseudocubic (Bricker, 1965) in morphology. The bixbyite product showed square holes (Figure 5e) and the hausmannite, rounded pseudocubes (Figure 5f) somewhat like those described by Bricker (1965). Thus, heated K- and Ba-birnessites formed hollandite-type structures, and Ni- and Mg-birnessites gave products with spinel structures.

The synthetic birnessite was compared with natural birnessites from Mexico and Japan, both of which were characterized by basal spacings of 7 Å. Traces of clay

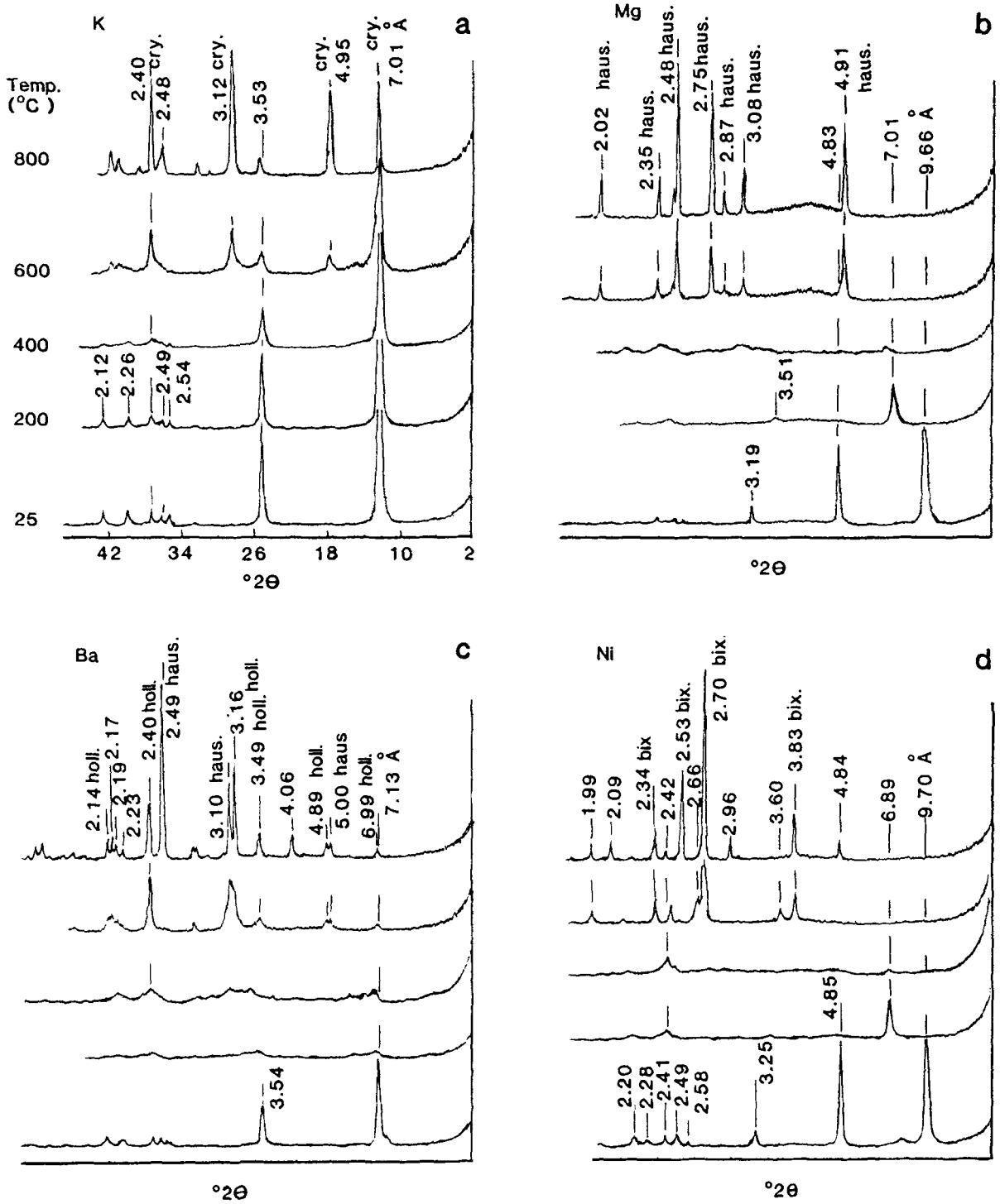

Figure 6. X-ray powder diffraction patterns of (a) heated K-birnessite composed primarily of cryptomelane; (b) heated Mg-birnessite composed of hausmannite; (c) heated Ba-birnessite composed of hollandite and hausmannite; (d) heated Ni-birnessite composed mostly of bixbyite.

https://doi.org/10.1346/CCMN.1986.0340503 Published online by Cambridge University Press

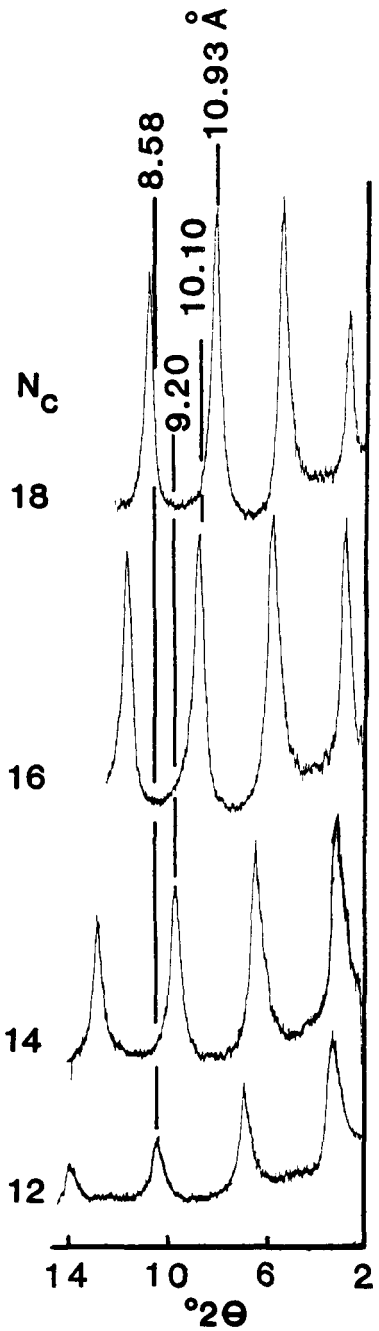

Figure 7. X-ray powder diffraction patterns of even-numbered C, n-alkylammonium birnessite samples (CuKα radiation).

minerals were present in both samples. Neither sample expanded on Mg saturation, and neither sample showed a high CEC. These properties are in accord with the above observation that the 7-Å form of birnessite is not expandable in the presence of cations such as Mn, K, Sr, La, and Ba, and possesses no cation-exchange properties. The natural samples on heating to 600°C formed bixbyite (data not shown) a behavior similar to the transition-metal-saturated synthetic birnessites.

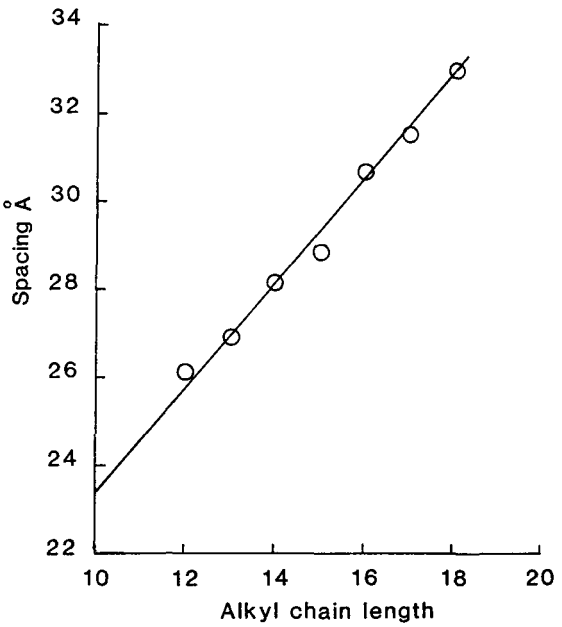

Figure 8. Plot of interlayer spacing (Å) vs. alkyl chain length for n-alkylammonium saturated birnessite samples.

Alkylammonium ion saturation

Synthetic Na-birnessite (7 Å) did not exchange with alkyl ammonium ions, whereas buserite (9.6 Å) exchanged interlayer metal ions with alkylammonium ions. Alkylammonium saturation produced a rational series of higher order XRD peaks, indicating the formation of ordered, alkylammonium complexes (Figure 7, Table 3). The basal spacing of the complex calculated from the third-order peak positions (Figure 7) increased linearly with the carbon chain length (Figure 8). This type of variation has also been observed for high-charge layer silicates (Lagaly and Weiss, 1969); however, the basal spacings of the alkylammonium derivatives of birnessite are larger than the values calculated by the procedure of Walker (1967). For vermiculite, the $-NH_3^+$ group probably sits in the hexagonal hole of the silicate layer, whereas in birnessite, no such hole exists in any of the proposed structures. Even after accounting for this difference, the basal spacing for a given alkylammonium ion seems to be larger for birnessite than for vermiculite. Arrhenius and Tsai (1981) proposed a structure with partial walls separating the MnO_6 sheets for birnessite as opposed to the one based on the structure of chalcophanite (Figure 1). The Arrhenius and Tsai structure explains the basal spacing obtained for alkylammonium-saturated birnessite, however, such partial walls were not found by high-resolution transmission electron micrographs (HRTEM) of ultrathin sections of alkylammonium

https://doi.org/10.1346/CCMN.1986.0340503 Published online by Cambridge University Press

Table 3. Basal spacings of birnessites saturated with alkylammoniom ions (in Å).

N_c[1]	Order of the X-ray diffraction peak			
	1st	2nd	3rd	4th
12	27.16	12.89	8.581	6.365
13	28.02	13.59	8.971	6.727
14	28.48	13.80	9.205	6.921
15	29.42	14.60	9.552	7.219
16	30.97	15.36	10.097	7.589
17	31.53	15.91	10.542	7.900
18	32.10	16.20	10.930	8.128

[1] Number of carbon atoms in the alkyl chain.

buserite (Paterson, 1981). The basal spacings of the alkylammonium buserite formed in our study could be fitted to the curve:

$$d(002) = 11.4 + 1.2n,$$

where n is the number of carbon atoms in the alkyl chain and d(002) represents the basal spacing in Å. The slope of the curve indicates that the carbon chains are at an angle of about 72° to the birnessite layer (Lagaly and Weiss, 1969). Lagaly (1982) derived the equation $d(002) = 11.0 + 0.98n$ for a vermiculite sample from Texas Mines Magnesite. These two equations have the same intercept, indicating that the effective thickness of the birnessite layer is close to that of vermiculite. Another possible explanation for such an increased layer thickness is the formation of alkylammonium birnessite of the type $[Mn_{14}O_{27}]^{-4} + [H_3N\text{-alkyl}^+]_4 \cdot 4H_2O$, where the interlayer spacing for the alkylammonium complex includes a layer of water in addition to alkyl ammonium ions. This complex is similar to that reported by Johns and Sen Guptha (1967) for alkylammonium-vermiculite $[(\text{vermiculite})^{-2.0} + (H_3N\text{-alkyl}^+)_2 \cdot 2H_2O]$. Continued evacuation and heating, however, did not collapse the birnessite complex any further, indicating the presence of strongly adsorbed water. No precautions were taken to avoid rehydration after mounting the sample on the goniometer. The behavior of alkylammonium-birnessite conforms to paraffin-type stacking of alkyl chains, which is characteristic of high-charge layer silicates (Lagaly and Weiss, 1969). Therefore, the formation of alkylammonium birnessite is in accord with the proposed layer structure of birnessite and its high CEC.

Oxidation of ferrous ions

Synthetic birnessite and natural manganese oxide minerals all oxidized solutions containing ferrous ions. The reaction produced iron oxide and dissolves the manganese oxide phase. Immersing a glass slide coated with birnessite in a solution of a dilute ferrous salt resulted in the precipitation of yellow-brown iron oxide and at the same time dissolved the birnessite. The pseudomorphic precipitate was probably ferrihydrite or feroxyhite which eventually aged to goethite.

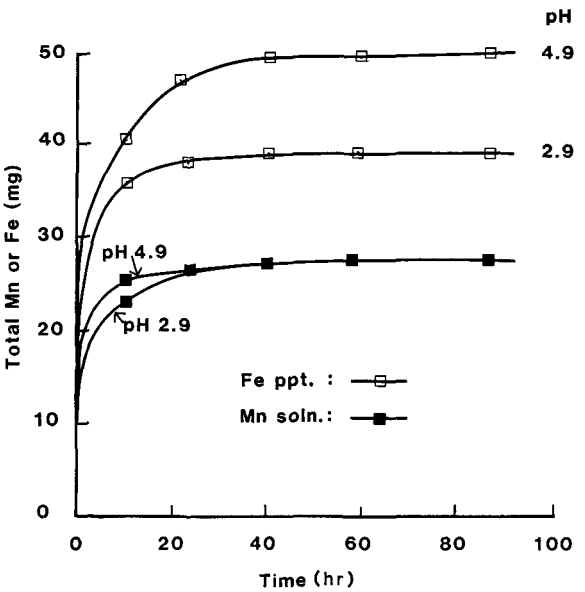

Figure 9. Total manganese released with time by Na-birnessite (50 mg) in a 0.01 M $FeSO_4$ solution (200 ml) at 25°C. ml) at 25°C.

Under controlled precipitation from ferrous sulfate solutions, $Fe(OH)_3$ formed at pH 2.9 and 4.9. Ferric hydroxide precipitation was complete at the latter pH due to the insolubility of $Fe(OH)_3$ species at pH 4.9. The relationship of Mn^{2+}-liberated to Fe^{3+}-precipitated is shown in Figure 9. Assuming a formula for soil birnessite of $(Na,Ca,Mg,Mn^{2+})Mn^{4+}{}_6O_{14} \cdot 6H_2O$ (Chukhrov and Gorshkov, 1981) and using only the cations Na and Mn^{2+} to balance the structural charge, the reaction with Fe^{2+} is written as:

$$12\ Fe^{2+}(aq) + Na_2Mn^{2+}Mn^{4+}{}_6O_{14} \cdot 6H_2O(s) + 28\ H^+ \rightarrow 12\ Fe^{3+}(aq) + 7\ Mn^{2+}(aq) + 2\ Na^+ + 20\ H_2O \quad (2)$$

and

$$Fe^{3+} + 3\ H_2O \rightarrow Fe(OH)_3 + 3\ H^+. \quad (3)$$

Oxidation of ferrous ions took place on the Mn-oxide surface or in interlayer positions. The Mn^{2+} ion resulting from reduction of Mn^{4+} moved into the solution phase, while the oxidized Fe^{3+} was hydrolyzed to form iron oxide [Eq. (3)]. The hydrolysis of Fe^{3+} was fast, and thus the shape of the birnessite particle was preserved by the iron oxide formed. For every Mn^{2+} ion released, about two iron atoms precipitated at pH 4.9. Inasmuch as all the air was not excluded from the reaction mixture, definite stoichiometry could not be established. The mechanism for formation of iron oxides in soil manganese nodules (McKenzie, 1986) requires rapid oxidation of Fe^{2+} in the presence of MnO_2, which accounts for the concentration of Fe-oxides in Mn-nodules under fluctuating oxidation-reduction conditions. The reactions studied here illustrate the feasibility of such a process.

https://doi.org/10.1346/CCMN.1986.0340503 Published online by Cambridge University Press

CONCLUSIONS

Synthetic sodium birnessite exhibited ion-exchange properties. Reversibility of exchange was dependent upon the nature of the cation and the drying treatment. When K-, Sr-, and La-birnessites were heated at 105°C, under vacuum for 12 hr, they underwent no ion exchange, whereas Li-, Na-, Ca-, and Ni-birnessite exchanged after similar treatment. The non-exchangeability and, hence, low CEC of natural birnessite is attributed to the presence of fixed cations.

Ion-exchanged birnessite showed variations in the *b* and *c* unit-cell dimensions; the *b* dimension increased with increase in size of the cation in birnessite. Alkylammonium ion saturation indicated the behavior of birnessite to be similar to that of vermiculite in accord with the high layer charge. The change in *b* dimensions with cation saturation and the change in *c* dimension upon alkylammonium saturation both showed similar trends to that observed for vermiculites. Alkylammonium data for Na-birnessite are in accord with a high-charge layer-structure model.

The Ba- and K-saturated birnessites at 600°C transformed to hollandite and cryptomelane, respectively. Birnessite saturated with Mg gave rise to hausmannite and Mn^{2+}- and Ni-birnessite gave rise to bixbyite. Heat transformations were influenced by the saturating cation.

The oxidizing power of Na-birnessite was indicated by its reaction with dilute ferrous sulfate at pH 2.9 and 4.9 to yield poorly crystalline iron oxide while itself being reduced to Mn^{2+}. A similar mechanism may operate in soil manganese nodules where poorly crystalline iron oxide coexists with Mn-oxide layers.

ACKNOWLEDGMENTS

The authors thank Nancy Lee for her help in preparing the manuscript and R. Giovanoli for generously providing his publications and synthesis procedures. We also thank F. A. Mumpton, R. G. Burns, and an anonymous reviewer for their valuable comments during the review process.

REFERENCES

Adams, S. N., Honeysett, J. L., Tiller, K. G., and Norrish, K. (1969) Factors controlling the increase of cobalt in plants following the addition of cobalt fertilizer: *Aust. J. Soil Res.* **7,** 29–42.

Arrhenius, G. O. and Tsai, A. G. (1981) Structure, phase transformation, and prebiotic catalysis in marine manganate minerals: *SIO Reference Series* **81-28,** Scripps Institution of Oceanography, La Jolla, California, 1–19.

Bricker, O. (1965) Some stability relations in the system $Mn\text{-}O_2\text{-}H_2O$ at 25° and one atmosphere total pressure: *Amer. Mineral.* **50,** 1296–1354.

Burns, R. G. and Burns, V. M. (1977) The mineralogy and crystal chemistry of deep-sea manganese nodules, a polymetallic resource of the twenty-first century: *Phil. Trans. R. Soc. Lond (A)* **286,** 283–301.

Chukhrov, F. V. and Gorshkov, A. I. (1981) Iron and manganese oxide minerals in soils: *Trans. Royal Society of Edinburgh* **72,** 195–200.

Embrey, P. G. and Fuller, J. P., eds. (1980) *A Manual of Mineral Names 1892–1978:* Oxford University Press, New York, p. 39.

Farmer, V. C. (1974) The layer silicates: in *The Infrared Spectra of Minerals,* V. C. Farmer, ed., Mineralogical Society, London, 331–363.

Giovanoli, R. and Balmer, B. (1981) A new synthesis of hollandite. A possibility for immobilization of nuclear waste: *Chimia* **35,** 53–55.

Giovanoli, R. and Brutsch, R. (1979) Über Oxihydroxide des Mn(IV) mit Schichtengitter. 5. Mitteilung: Stoichiometrie, Austauschverhalten und die Rolle bei der Bildung von Tiefsee-Mangankonkretionen: *Chimia* **33,** 56–60.

Giovanoli, R., Buhler, H., and Sokolowska, K. (1973) Synthetic lithiophorite: electron microscopy and X-ray diffraction: *J. Microscopie* **18,** 271–284.

Giovanoli, R., Stähli, E., and Feitknecht, W. (1970) Über Oxihydroxide des vierwertigen Mangans mit Schichtengitter 1. Natrium-Mangan(II, III) Manganat(IV): *Helv. Chim. Acta* **53,** 209–220.

Johns, W. D. and Sen Guptha, P. K. (1967) Vermiculite-alkylammonium complexes: *Amer. Mineral.* **52,** 1706–1724.

Lagaly, G. (1982) Layer charge heterogeneity in vermiculites: *Clays & Clay Minerals* **30,** 215–222.

Lagaly, G. and Weiss, A. (1969) Determination of the layer charge in mica-type layer silicates: in *Proc. Int. Clay Conf., Tokyo, 1969, Vol. 1,* L. Heller, ed., Israel Univ. Press, Jerusalem, 61–80.

Loganathan, P. and Burau, R. G. (1973) Sorption of heavy metal ions by a hydrous manganese oxide: *Geochem. Cosmochim. Acta* **37,** 1277–1293.

Mason, B. and Berry, L. G. (1968) *Elements of Mineralogy:* Freeman, San Francisco, 552 pp.

McKenzie, R. M. (1967) The sorption of cobalt by manganese minerals in soils: *Aust. J. Soil Res.* **8,** 97–106.

McKenzie, R. M. (1986) Manganese oxides and hydroxides: in *Minerals in Soil Environments, 2nd ed.,* J. B. Dixon and S. B. Weed, eds., Soil Science Society of America, Madison, Wisconsin (in press).

Paterson, E. (1981) Intercalation of synthetic buserite by dodecylammonium chloride: *Amer. Mineral.* **66,** 424–427.

Potter, R. M. and Rossman, G. R. (1979) The tetravalent manganese oxides: identification, and structural relationships by infrared spectroscopy: *Amer. Mineral.* **64,** 1199–1218.

Ruehlicke, G. and Kohler, E. E. (1981) A simplified procedure for determining layer charge by the N-alkylammonium method: *Clay Miner.* **16,** 305–307.

Stähli, E. (1968) Über Manganate(IV) mit Schichten-Struktur: Ph.D. Thesis, University of Bern, Switzerland, 37 pp.

Taylor, R. M., McKenzie, R. M., and Norrish, K. (1964) The mineralogy and chemistry of manganese in some Australian soils: *Aust. J. Soil Res.* **2,** 235–248.

Walker, G. F. (1967) Interaction of n-alkylammonium with mica-type layer lattices: *Clay Miner.* **7,** 129–143.

Weed, S. B. and Weber, J. B. (1968) The effect of adsorbent charge on the competitive adsorption of divalent organic cations by layer silicate minerals: *Amer. Mineral.* **53,** 478–490.

Wilding, L. P., Smeck, N. E., and Drees, L. R. (1977) Silica in soils: quartz, cristobalite, tridymite, and opal: in *Minerals in Soil Environments,* J. B. Dixon and S. B. Weed, eds., Soil Science Society of America, Madison, Wisconsin, 471–552.

(Received 3 September 1985; accepted 27 January 1986; Ms. 1514)